Revista Mexicana de Astronomía y Astrofísica, **35**, 45–63 (1999)

WEAK RADIO GALAXIES. II. NARROW-BAND OPTICAL IMAGING AND PHYSICAL CONDITIONS[1]

R. Carrillo and I. Cruz-González

Instituto de Astronomía
Universidad Nacional Autónoma de México

and

J. Guichard

Instituto Nacional de Astrofísica, Optica y Electrónica
Tonantzintla, Pue., México

Received 1998 October 27; accepted 1999 February 24

RESUMEN

Se presenta un estudio de las regiones extendidas con líneas en emisión de 26 radiogalaxias débiles en Hα y [O III]. Se detecta emisión en todas las galaxias y en 81% se resuelven regiones extendidas con tamaños promedio de 4.6 kpc. Las morfologías son predominantemente ovaladas o elípticas con condensación central de 1 kpc y en algunos casos hay estructuras filamentarias a varios kpc del núcleo. Sólo en B2 1346+26 se detectan dos lóbulos de gas ionizado que coinciden espacialmente con los observados en radio frecuencias. En el resto la EELR está asociada a la estructura de la fuente central en radio. Las estimaciones de luminosidades, densidad y masa del gas ionizado de las radiogalaxias débiles son similares a las de las potentes. Se propone que también en las radiogalaxias débiles, la fuente central es responsable de la ionización del gas, y que el gas observado ha sido adquirido por fusión o interacción de galaxias con al menos una de éstas rica en gas.

ABSTRACT

The study of the extended emission-line regions of 26 weak radio galaxies is presented. Emission is detected in all galaxies and extended regions are resolved in 81%, with mean sizes of 4.6 kpc. Morphologies are predominantly oval or elliptical with a central condensation of kpc in size and in some cases there are filamentary structures at several kpc from the nucleus. Just in B2 1346+26 two lobes of ionized gas are detected that spatially coincide with those observed in radio frequencies. In the remaining sources the EELR is associated to the structure of the radio core region. The estimated luminosities, density and mass of the ionized gas of the weak radio galaxies are similar to those of powerful ones. It is proposed that also in weak radio galaxies the central source is responsible of the gas ionization and that the observed gas has been acquired by mergers or interaction of galaxies, with at least one of them rich in gas.

Key words: **GALAXIES – ACTIVE — GALAXIES – INTERACTIONS — GALAXIES – NUCLEI**

[1] Based on observations collected at the Observatorio Astronómico Nacional, San Pedro Mártir, B. C., México.

1. INTRODUCTION

The properties of extended emission-line regions (hereafter, EELR) in powerful radio galaxies (PRGs), with $S_{408\,Mhz} \geq 8.5$ Jy, has been studied by Baum & Heckman (1989a,b). In a sample of 43 sources they resolved EELR in $\sim 85\%$ of the cases, with sizes of tens of kpc and with a variety of morphologies. Some sources are small, centrally condensed and roughly symmetric about the host galaxy nuclei, often with roughly oval or elliptical shapes; while in others, there are extended filaments at several kpc from the nucleus. The average emission-line luminosities in Hα+[N II] or [O III], are 3×10^{41} erg s^{-1} (Baum et al. 1988; Baum & Heckman 1989a,b). In the case of B2 radio galaxies, the presence of the EELR in B2 1346+26 (4C 26.42) has been studied by van Breugel, Heckman, & Miley (1984). In this source, the EELR is morphologically related to the radio continuum distribution, occurring predominantly along the radio source boundary, the brightness increases near an indentation and is enhanced at the central radio source. Similar results have been found in other radio sources (e.g., 3C 277.3, van Breugel et al. 1985).

In Paper I (Carrillo, Cruz-González, & Guichard 1997), we reported a study of the optical properties of weak radio galaxies (WRGs) selected from the second Bologna survey (B2). It contains broad-band optical CCD images of 30 radio galaxies obtained at V, R, and I. We presented the morphological and photometric results (surface photometry, colors, and intensity profiles), and found that most WRGs are elliptical galaxies with peculiar morphologies, usually located in high galaxy density environments.

In this paper we present a follow-up narrow-band imaging study of 26 WRGs, in an attempt to resolve their extended emission-line regions. The images include narrow-band data at both Hα+[N II] and [O III], obtained at the corresponding galaxy redshifts.

The principal goals in our study of weak radio galaxies (WRGs) focus on the understanding of the following questions: (1) What is the frequency of EELR in weak radio galaxies? and how it compares to powerful radio galaxies? (2) What is the origin of the gas in the EELR in WRGs: tidal interactions (or mergers) with companion galaxies and/or thermal instabilities in a hot, diffuse interstellar or intergalactic medium? (3) What is the spatial relationship between the EELR and the radio structure, and between the EELR and the broad-band optical host galaxy? (4) The origin of the photoionization is due to the central source or/and external sources (shocks)? (5) What is the effect of the possible interactions in the radio structure and the morphological properties of the EELR? (6) What are the implications of our results in the unification scenario for radio galaxies?

TABLE 1

CHARACTERISTICS OF FILTERS USED

	Hα		[O III]	
Δz	λ_c^a	$\Delta\lambda^a$	λ_c^a	$\Delta\lambda^a$
$0 \rightarrow 0.011$	6607	89	5028	71
$0.012 \rightarrow 0.026$	6690	91	5121	71
$0.031 \rightarrow 0.044$	6819	86	5199	71
$0.048 \rightarrow 0.061$	6920	88	5291	75
$0.061 \rightarrow 0.075$	7027	93	5366	78

[a] In Å.

The paper is organized as follows, § 2 contains a description of the observations and sample. The image analysis procedures are described in § 3. The photometric and morphological results are presented in § 4, followed by a discussion of the EELR properties in WRGs in § 5, and individual galaxy descriptions in § 6. Finally, § 7 contains a summary of our results and conclusions.

2. OBSERVATIONS

2.1. *Sample Selection*

The observed sample consists of 26 galaxies identified with radio sources of the Second Bologna Survey (B2) (for details see Fanti et al. 1987). Radio studies of these galaxies provided us with information about radio luminosities, morphological properties, and jet properties. The selected galaxies satisfy the criteria presented in Paper I and all, except one, have broad-band images from our work.

2.2. *Instrumentation*

The observations were carried out at the 2.12-m telescope of the Observatorio Astronómico Nacional at San Pedro Mártir (OAN/SPM), B. C., México, during several observing runs: March, June, July, and October 92, April and September 93. CCD images were taken using Hα+[N II] $\lambda\lambda$6548,6583 and [O III] λ5007 narrow-band filters. Since the observed galaxies have different redshifts, the central wavelength and bandpass of the filters used for each redshift interval are presented in Table 1.

A Thompson 1024 × 1024 CCD detector with a read-out noise of 5.73 e^{-1} and 19 μm of pixel size was used. This detector and the f/7.5 secondary yield an image scale in the focal plane of 0.25″/pixel and a field of view of 4.25′ × 4.25′. The typical seeing for the observations was in the range from 1.0 to 2.4″.

The details of the narrow-band galaxy observations are presented in Table 2, which includes the source name, observing dates, filters, integration time, and the image quality (PSF).

TABLE 2

Hα+[N II] AND [O III] OBSERVATIONS

Source B2	Obs. Date	Fil.	Integ. Time	PSF FWHM	Obs. Date	Fil.	Integ. Time	PSF FWHM
0034+25	93 Sep	$H\alpha_z^a$	1200^s	1.5″	93 Sep	$[O\ III]_z^a$	1800^s	1.6″
	...	$H\alpha_c^b$	1200	1.7	...	$[O\ III]_c^b$	1200	1.5
0055+26	92 Oct	$H\alpha_z$	1800	1.7	92 Oct	$[O\ III]_z$	3600	1.9
	...	$H\alpha_c$	1800	1.8	...	$[O\ III]_c$	3600	1.9
0116+31	93 Sep	$H\alpha_z$	1800	1.7	92 Oct	$[O\ III]_z$	3600	1.7
	...	$H\alpha_c$	1800	1.5	...	$[O\ III]_c$	3600	1.7
0120+33	93 Sep	$H\alpha_z$	1800	1.6	93 Sep	$[O\ III]_z$	2700	1.8
	...	$H\alpha_c$	1800	1.9	...	$[O\ III]_c$	2700	2.3
0331+39	93 Sep	$H\alpha_z$	1800	1.6	93 Sep	$[O\ III]_z$	2400	1.6
	...	$H\alpha_c$	1200	1.5	...	$[O\ III]_c$	2400	1.7
0838+32	...	...	...	...	92 Oct	$[O\ III]_z$	2700	1.8
	...	...	...	...	...	$[O\ III]_c$	1800	1.9
0913+38	...	...	...	...	93 Apr	$[O\ III]_z$	3600	2.5
	...	...	...	...	...	$[O\ III]_c$	3600	2.1
0916+33	92 Oct	$H\alpha_z$	1200	2.2	92 Oct	$[O\ III]_z$	1800	2.3
	...	$H\alpha_c$	900	1.8	...	$[O\ III]_c$	1800	2.0
1116+28	92 Mar	$H\alpha_z$	900	1.9	93 Apr	$[O\ III]_z$	1800	2.3
	...	$H\alpha_c$	900	1.5	...	$[O\ III]_c$	1800	1.8
1144+35	92 Mar	$H\alpha_z$	900	1.0	...	...	...	...
	...	$H\alpha_c$	900	1.1	...	...	...	...
1322+36	...	...	...	...	93 Apr	$[O\ III]_z$	2400	1.8
	...	...	...	...	...	$[O\ III]_c$	2400	1.7
1339+26	93 Mar	$H\alpha_z$	1200	2.1	...	...	...	...
	...	$H\alpha_c$	900	1.8	...	...	...	...
1346+26	93 Mar	$H\alpha_z$	180	2.0	...	...	...	...
	...	$H\alpha_c$	300	1.7	...	...	...	...
1357+28	...	...	...	...	93 Apr	$[O\ III]_z$	3600	1.6
	...	...	...	...	...	$[O\ III]_c$	2100	1.8
1422+26	92 Jun	$H\alpha_z$	300	2.0	...	...	...	...
	...	$H\alpha_c$	300	1.8	...	...	...	...
1441+26	...	...	...	...	93 Apr	$[O\ III]_z$	2400	1.8
	...	...	...	...	...	$[O\ III]_c$	2400	1.9
1557+26	92 Jul	$H\alpha_z$	900	1.8	93 Apr	$[O\ III]_z$	2400	1.9
	...	$H\alpha_c$	900	1.9	...	$[O\ III]_c$	2400	1.7
1652+39	93 Mar	$H\alpha_z$	900	2.0	93 Apr	$[O\ III]_z$	2700	1.7
	...	$H\alpha_c$	900	2.3	...	$[O\ III]_c$	2700	1.5
1658+30	92 Jun	$H\alpha_z$	300	2.0	93 Apr	$[O\ III]_z$	3300	1.7
	...	$H\alpha_c$	300	1.8	...	$[O\ III]_c$	2700	1.7
1752+32	...	...	...	...	93 Apr	$[O\ III]_z$	3600	2.0
	...	...	...	...	...	$[O\ III]_c$	3600	2.0
1833+32	...	...	...	...	93 Apr	$[O\ III]_z$	3600	1.7
	...	...	...	...	.....	$[O\ III]_c$	3600	1.8

TABLE 2 (CONTINUED)

Source B2	Obs. Date	Fil.	Integ. Time	PSF FWHM	Obs. Date	Fil.	Integ. Time	PSF FWHM
1855+37	93 Sep	$H\alpha_z$	1800	1.5	...	...	...	...
	...	$H\alpha_c$	1800	1.8	...	...	...	...
2116+26	92 Oct	$H\alpha_z$	1200	1.9	92 Oct	$[O\ III]_z$	1800	1.7
	...	$H\alpha_c$	1200	2.0	...	$[O\ III]_c$	1800	1.8
2236+35	93 Sep	$H\alpha_z$	1800	2.1	93 Sep	$[O\ III]_z$	2700	1.9
	...	$H\alpha_c$	1800	2.0	...	$[O\ III]_c$	2700	2.2
2320+32	93 Sep	$H\alpha_z$	1800	1.5	93 Sep	$[O\ III]_z$	1800	1.9
	...	$H\alpha_c$	1200	1.6	...	$[O\ III]_c$	1800	1.6
2335+26	...	...	...	...	92 Oct	$[O\ III]_z$	2700	1.8
	...	...	...	...	...	$[O\ III]_c$	2700	2.0

[a] z Filter at redshift of the source.
[b] c Filter at continuum.

2.3. *Photometric Observations*

A set of standard stars from the list of Oke (1974), were acquired each night for photometric calibrations: GD 140 and L 970–30 (March 1992), L 970–30 (June 1992), Hz 29 (July 1992), BD +40 4032, Feige 24 and He 3 (October 1992), BD +8 2015, L 930–80 and Wolf 485A (April 1993), and BD +28 4211 and G 191B2B (September 1993).

3. IMAGE ANALYSIS

The reduction of the two-dimensional CCD frames follows the standard procedures (e.g., Kent 1984; Cornell et al. 1987), using the flat field and bias images obtained each night. The NOAO Image Reduction and Analysis Facility (IRAF) software was used. The general reduction procedure was presented in Paper I. To obtain the final line-emission and photometric calibration images, the adopted procedure was the following:

1. Two sets of various galaxy images were taken for each filter, one at source redshift (ON) and another at the continuum (OFF).
2. Each set of images (ON and OFF) were combined and aligned, so that the final images (ON and OFF) result from the combination of at least 4 frames.
3. The final emission-line image was obtained by subtracting the continuum or stellar contribution (ON – OFF), taking into account the width of the filters used.
4. The final images were deconvolved with the Lucy-Richardson algorithm (Lucy 1974; Richardson 1972) and smoothed with a bi-dimensional Gaussian (e.g., see Fabbiano, Fassnacht, & Trinchieri 1994).
5. To calibrate the flux photometrically, standard star images were obtained at Hα+N II and [O III] from the list of Oke (1974).

4. PHOTOMETRIC AND MORPHOLOGICAL RESULTS

4.1. *Images*

The final images of the WRGs with EELR are presented in Figures 1*a* and 1*b*, and contour maps in Figures 2*a* and 2*b*, corresponding to the narrow-filters Hα+[N II] $\lambda\lambda$6548,6583 or [O III] λ5007. In Figures 3*a* and 3*b*, we present overlays of the radio emission maps and the observed EELR.

We found that most sources have EELR with morphologies that are usually oval or elliptical with outer contours usually distorted. Most have centrally condensed structures associated to the nuclei of the host galaxies. Some galaxies show double or even multiple components in either a common halo or separated structures. In some cases, extended filament- or tail-like structures are detected. A description of the EELR of individual galaxies studied here is presented below (§ 6). In Figure 4, the galaxy B2 1346+26 EELR is compared to the radio continuum map (van Breugel et al. 1984) and the dust lane image (Pinkney et al. 1996).

4.2. *Properties of Extended Emission-Line Gas*

From the photometric calibrated emission-line images, we obtained for each galaxy the following parameters: the total intensity of the emission at Hα+[N II] and [O III], the size and the position angle of the EELR. The sizes of the emitting regions

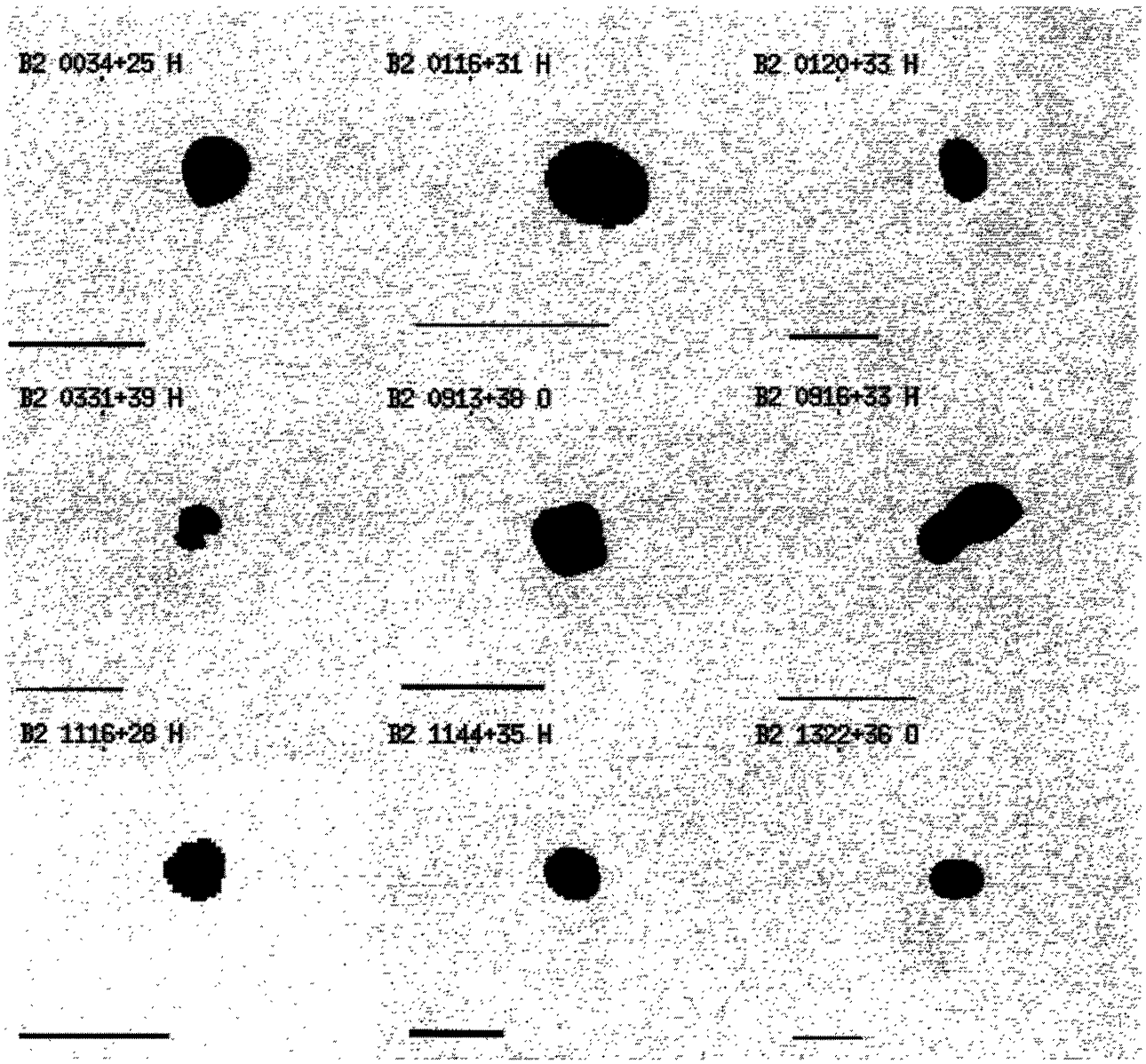

Fig. 1*a*. EELR images in Hα (H in image) or [O III] (O in image) of B2 radio galaxies. North is up and east is to the left. The bar corresponds to 15″.

correspond to the radius at half maximum intensity, while the position angles (PA) of the major axis are measured counterclockwise from the north.

In Table 3 the derived fluxes and luminosities (assuming $H_0 = 100$ km s^{-1} Mpc^{-1}) for each galaxy are presented, while Table 4 includes the size and PA of the emitting regions.

We establish that spatially extended emission-line gas is quite common in weak radio galaxies. We detected line emission in Hα+[N II] and/or [O III] from all galaxies in the sample, but in some cases it is unresolved. In $\sim$ 81% of the studied WRGs we have resolved the line emitting region with sizes between 1.6 and 9.1 kpc. The observed structure shows usually a central concentration, associated to the core source of the radio emission and the host galaxy nucleus, surrounded by oval or elliptical structures. In most cases, the emission in the outer zones is clearly

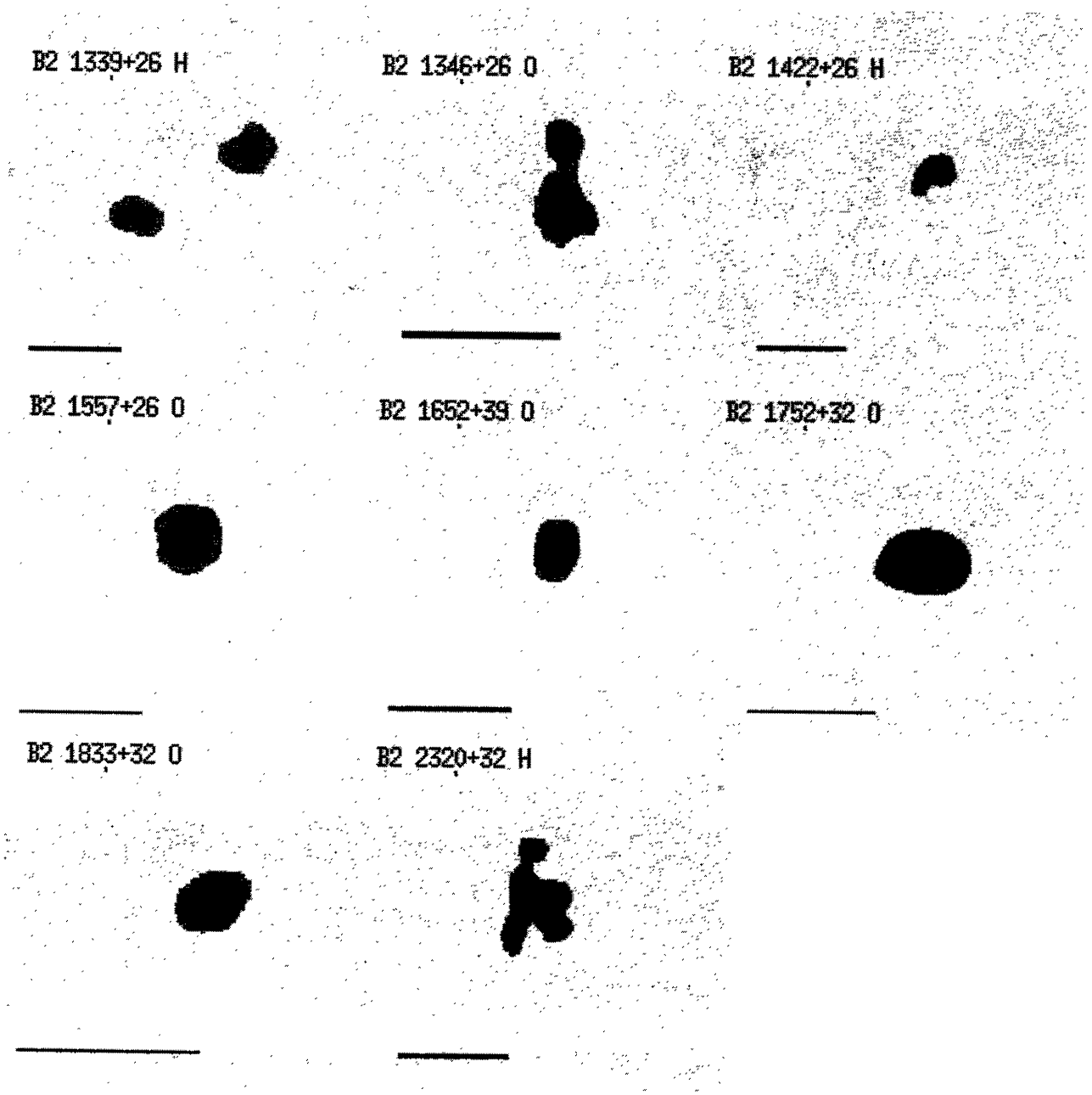

Fig. 1*b*. EELR images in Hα (H in image) or [O III] (O in image) of B2 radio galaxies. North is up and east is to the left. The bar corresponds to 15″.

distorted, sometimes due to the presence of companions or inherent to the complexity of the emitting region.

5. DISCUSSION

5.1. *Characteristics of EELR*

The percentage of EELR in WRGs that we have obtained and their morphologies are very similar to those found in PRGs by Baum et al. (1988), i.e., $\sim$ 85% in 38 sources. These results show that ionized emitting gas can be present in the host galaxies of radio galaxies, independently of their radio power. The difference between the EELR of WRGs and PRGs are smaller mean size and emission-line luminosity (Hα+[N II] and/or [O III]): in PRGs the mean radius is $\sim$ 10 kpc (Hansen, Nørgaard-Nielson, & Jørgensen 1987; Baum et al. 1988) and the mean

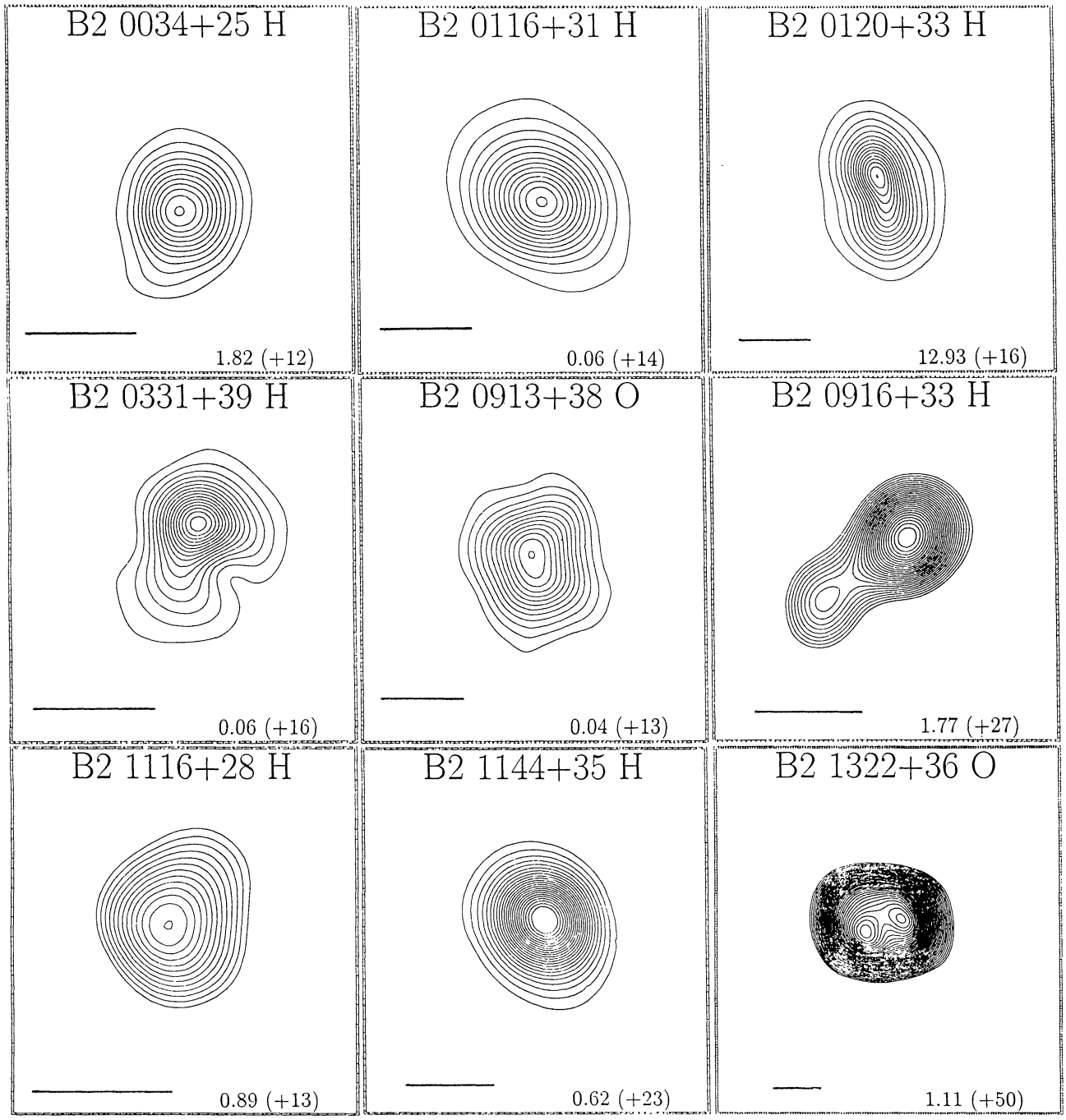

Fig. 2*a*. EELR contour plots in Hα (H in figure) or [O III] (O in figure) of B2 radio galaxies. North is up and east is to the left. The bar corresponds to 5″. The contour levels are given at the down right of center; the first number is the peak flux (in 10^{-2} mJy); and the number in parenthesis is the number of successive linear contour levels.

emission-line luminosity is $\sim 3 \times 10^{41}$ erg s^{-1}, with values from 2.2×10^{39} to 1.3×10^{43} erg s^{-1} (Baum & Heckman 1989a); while in WRGs the mean size is 4.6 kpc and the mean emission-line luminosity is $\sim 1 \times 10^{41}$ erg s^{-1} with values from 1.3×10^{39} to 6.7×10^{41} erg s^{-1}. The sizes of WRGs line-emission regions are similar to those of Seyfert galaxies ($\sim$ 4 kpc) and luminosities are somewhat higher ($\sim 6.5 \times 10^{39}$ erg s^{-1}), as reported by Pogge (1989). We conclude that the EELR dimensions and luminosities are possibly linked to the central source power.

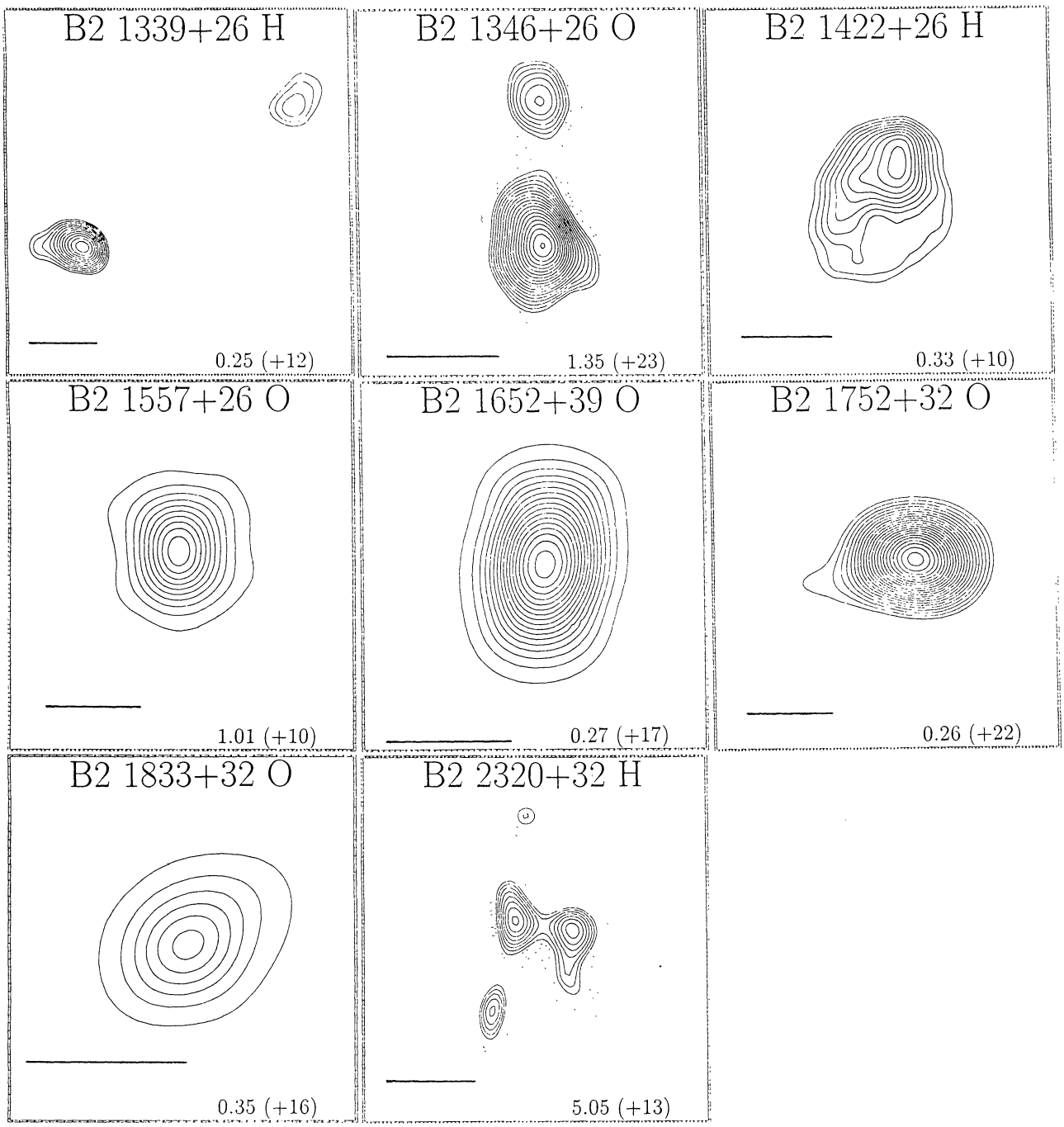

Fig. 2*b*. EELR contour plots in Hα (H in figure) or [O III] (O in figure) of B2 radio galaxies. North is up and east is to the left. The bar corresponds to 5″. The contour levels are given at the down right of center; the first number is the peak flux (in 10^{-2} mJy), and the number in parenthesis is the number of successive linear contour levels.

The observed differences in mean radius and luminosities of the EELR in different AGNs can be the result of a major capacity of ionization from the radio core in PRGs or/and to the efficiency of shocks between the radio structure and the intergalactic gas of the host galaxy. These options are possible since PRGs have a core with high radio luminosity and powerful radio jets with sizes from kpc to Mpc that could influence the intergalactic gas more efficiently, while sources of less activity produce smaller emitting regions and jets, and are less luminous, producing weaker shocked regions.

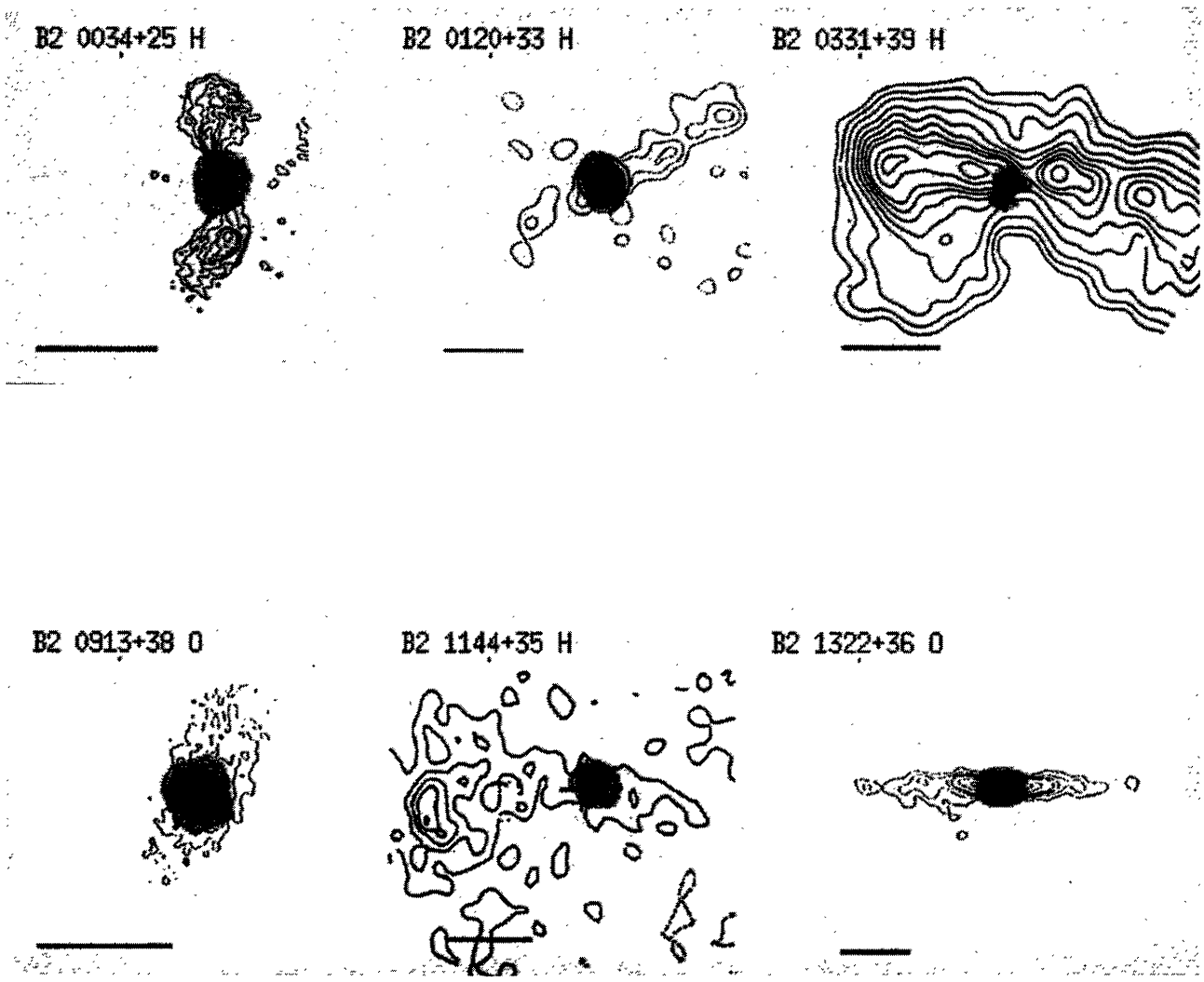

Fig. 3*a*. Overlay of radio emission contours (from Bologna group papers, see § 5.3) in the Hα (H in image) or [O III] (O in image) images of EELR. North is up and east is to the left. The bar corresponds to 15″.

5.2. *Physical Parameters of the EELR*

To compare the physical properties of the EELR in different types of radio galaxies (PRGs and WRGs), we need to derive n_e (electron density), M_{gas} (mass of gas in the EELR), and U (ionization parameter). We used the relations presented by Baum & Heckman (1989a) for case B recombination

$$n_e^2 = \frac{L_{\mathrm{H}\alpha}}{f\ V\ \alpha_{\mathrm{H}\alpha}^{eff}\ h\ \nu_{\mathrm{H}\alpha}}\ , \qquad (1)$$

$$M_{gas} = f\ V\ n_e\ m_p\ = \frac{L_{\mathrm{H}\alpha}\ m_p}{\alpha_{\mathrm{H}\alpha}^{eff}\ h\ \nu_{\mathrm{H}\alpha}\ n_e}\ , \qquad (2)$$

$$U = \frac{Q_H}{4\pi r^2\ n_e\ c} = \frac{1}{4\pi r^2\ n_e\ c}\frac{2.2\ L_{\mathrm{H}\alpha}}{h\ \nu_{\mathrm{H}\alpha}}\ . \qquad (3)$$

In these relations $L_{\mathrm{H}\alpha}$ is the Hα luminosity from the portion of the nebulae for which the density is being estimated, V is the volume occupied by the emitting gas, f is the volume filling factor in the gas, h is Planck's constant, c the speed of light, $\nu_{\mathrm{H}\alpha}$ is the frequency of the Hα line, $\alpha_{\mathrm{H}\alpha}^{eff} = 1.17 \times 10^{-13}$ cm^3 s^{-1} is the effective coefficient of recombination (Brocklehurst 1971), and Q_H is the number of ionizing photons per second emitted by the active nucleus. We assume a filling factor $f = 1$ and so, the derived values are lower limits for n_e, and upper limits for M_{gas} and U.

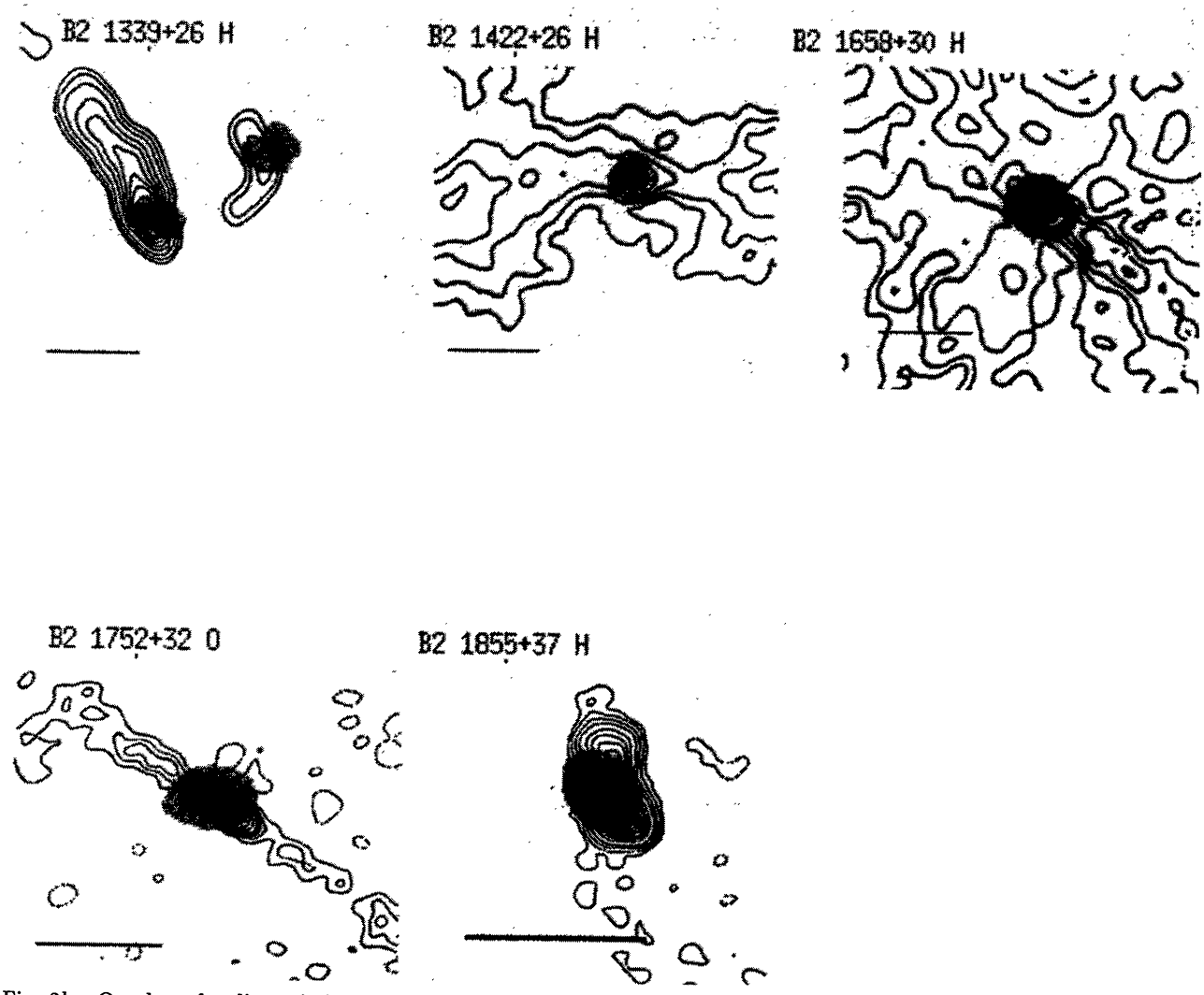

Fig. 3*b*. **Overlay of radio emission contours (from Bologna group papers, see § 5.3) in the Hα (H in image) or [O III]** (O in image) images of EELR. North is up and east is to the left. The bar corresponds to 15″.

Since our emission-line images contain emission from either Hα+[N II] or [O III], to estimate $L_{\mathrm{H}\alpha}$ alone, we need to assume appropriate line ratios for [N II] and [O III]

$$\frac{[\mathrm{N\ II}]\ \lambda6548 + [\mathrm{N\ II}]\ \lambda6583}{\mathrm{H}\alpha} \sim 1.3 \pm 0.8 \ , \quad (4)$$

$$\frac{[\mathrm{O\ III}]\ \lambda5007}{\mathrm{H}\alpha} \sim 0.9 \pm 0.7 \ , \quad (5)$$

as proposed by Costero & Osterbrock (1977), Koski (1978), and Osterbrock & Miller (1975).

With the $L_{\mathrm{H}\alpha}$ values we estimated the ionization gas parameters for the WRGs presented in Table 4. The derived values of the electron density range from 0.01 to 0.26 cm^{-3}, the mass in emission-line gas from 1.16×10^8 to 2.63×10^9 $M_\odot$ and the ionization parameter from 0.05×10^{-2} to 1.06×10^{-2}. Mean values for the WRG sample are $< n_e > = 0.09$ cm^{-3}, $< M > = 9.23 \times 10^8$ $M_\odot$ and $< U > = 0.40 \times 10^{-2}$.

The WRGs ionized gas parameters are within the values found in PRGs (Baum & Heckman 1989a): $n_e = 0.05$ to 0.5 cm^{-3}; $M = 4 \times 10^7$ to 6×10^9 $M_\odot$ and $U = 0.03 \times 10^{-2}$ to 4×10^{-2}. We conclude that the ionized gas in weak and powerful radio galaxies are similar.

5.3. *Energetic Correlations*

In Table 5 we list the Hα luminosities, using line ratios given by (4) and (5) that correspond to the to-

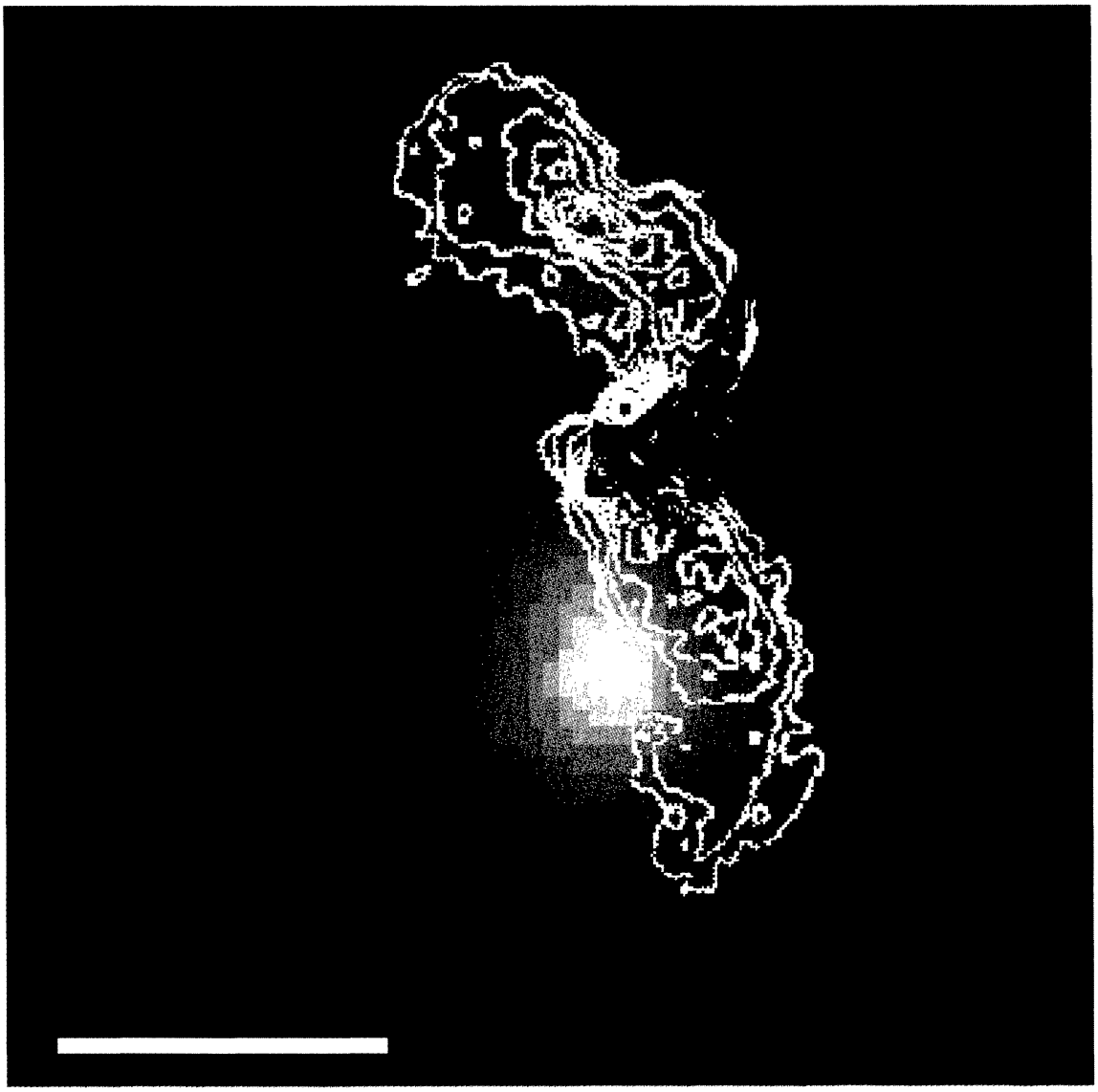

Fig. 4. B2 1346+26 color representation of the [O III] λ5007 line emission overlayed with radio emission contours at 6 cm (van Breugel et al. 1984) and the dust lane found by Pinkney et al. 1996 (blue contours). The bar corresponds to 5″, orientation as in Figure 1*a*.

tal line-emitting region in our images, together with the radio luminosities (total and core) given by the Bologna group (Parma et al. 1986; de Ruiter et al. 1986; Fanti et al. 1986, 1987; Morganti et al. 1987; Parma et al. 1987; Capetti et al. 1993).

In Figures 5*a* and 5*b*, we compare the total radio luminosity and the radio core luminosity with $L_{\mathrm{H}\alpha}$, respectively. A possible linear correlation between the radio continuum and the emitting gas luminosities is shown, but the dispersion in these plots is large. The slopes of the correlations are: 0.22 ± 0.07 (total radio luminosity) and 0.11 ± 0.07 (radio core luminosity). These values are consistent with the 0.28 ± 0.07 slope found by Zirbel & Baum (1995) for FRI sources.

To compare our WRG results with different types of AGNs, we present L_{radio}^{total} and $L_{\mathrm{H}\alpha}$ in Figure 6 for PRGs (Baum & Heckman 1989a), WRG (this paper), radio-loud steep-spectrum QSOs (Stockton & Mac Kenty 1987), high-redshift radio sources (Spinrad 1987) and Seyfert galaxies (de Bruy & Wilson 1978; Whittle 1985). The energetic sequence shown here was previously discussed by Baum & Heckman (1989a,b) and the existence of a unique relation for different types of AGNs is still controversial (Morganti, Ulrich, & Tadhunter 1992; Zirbel & Baum

TABLE 3

Hα[a] AND [O III] FLUX AND LUMINOSITY

Source B2	$F_{H\alpha}$ (10^{-2}mJy)	$L_{H\alpha}$ (10^{40}erg s^{-1})	$F_{[OIII]}$ (10^{-2}mJy)	$L_{[O\ III]}$ (10^{40}erg s^{-1})
0034+25	1.82	9.50	0.28	1.94
0055+26	5.85	66.94	1.97	29.51
0116+31	0.06	0.99	0.79	18.84
0120+33	12.93	17.34	4.07	7.15
0331+39	0.06	0.13	0.12	0.33
0838+32	...	...	0.20	6.22
0913+38	...	...	0.04	1.26
0916+33	1.77	22.80	1.26	21.31
1116+28	0.89	20.76	1.51	45.96
1144+35	0.62	12.74	...	...
1322+36	...	...	1.11	15.32
1339+26	0.25	6.14	...	...
1346+26	1.35	28.22	...	...
1357+28	...	...	0.14	3.83
1422+26	0.33	2.31	...	...
1441+26	...	...	0.04	0.92
1557+26	0.80	7.98	1.01	13.30
1652+39	1.50	8.64	0.27	2.04
1658+30	1.76	11.03	1.38	11.30
1752+32	...	...	0.26	3.49
1833+32	...	...	0.35	8.17
1855+37	0.02	0.26	...	...
2116+26	0.50	0.68	0.42	0.74
2236+35	0.37	1.44	0.09	0.46
2320+32	5.05	7.89	1.78	3.64
2335+26	...	...	0.28	1.68

[a] Filter includes the Hα and [N II] lines.

1995; Baum, Zirbel & O'Dea 1995). Our addition to this plot are measured values of $L_{H\alpha}$ for WRGs. The WRGs, as noted by Zirbel & Baum (1995) and Baum et al. (1995), have a flatter slope than the rest of radio galaxies. We note that Seyfert galaxies and WRGs in this plot share a common region. Morganti et al. (1992) favor a unique sequence with a slope of 0.54 ± 0.02. In their context the addition of WRGs to the rest of AGNs yields a tight correlation (r = 0.82) with slope 0.59 ± 0.14 and b = 15.96 ± 1.57. This can be easily explained with the contribution of the WRGs flatter slope (0.22 ± 0.07, this work) and the PRGs steep slope (0.75 ± 0.09, Zirbel & Baum 1995). The turnover discussed by Zirbel & Baum (1995) is also clearly shown in Fig. 6, where WRGs show much more $L_{H\alpha}$ than expected if the PRGs relation is applicable. The observed $L_{H\alpha}$ values in WRGs produce ≈ 100 times less radio luminosity than the PRGs with comparable line luminosities.

In Figure 7, the radio core and Hα luminosities for radio galaxies (PRG and WRG) are compared. The correlation in this case: log $L_{H\alpha}$ = m log L_{radio}^{core} + b, yields m = 0.87 ± 0.09 and b = 15.79 ± 1.55 (r = 0.60).

The relation between the radio luminosity and the Hα luminosity has various explanations. If we assume that the radio core is directly responsible of the activity in all sources, then the radio core seems also responsible of the bulk of the ionization of the emitting gas. However, the dispersion observed can be due to the shock interaction between radio jets and the intergalactic gas and dust from the host galaxy, in this case the EELR is being ionized by both a power-law and shocks; as proposed by some models of the NLR (Narrow Line Regions) in AGNs (e.g.,

TABLE 4

PHYSICAL CONDITIONS OF EELR IN WRGs

Source B2	Size[a] (kpc)	PA (o)	n_e (cm^{-3})	M_{gas} ($10^8\ M_\odot$)	U (10^{-2})
0034+25	3.2	3	0.10	9.91	0.40
0055+26	6.2^p	152	0.26	26.30	1.06
0116+31	3.6	79	0.15	14.71	0.60
0120+33	2.0	21	0.13	13.39	0.54
0331+39	3.0	165	0.01	1.16	0.05
0838+32	unr.	...	0.08	8.45	0.34
0913+38	5.0	24	0.04	3.80	0.15
0916+33	4.6	137	0.15	15.35	0.62
1116+28	...	45	0.15	14.65	0.59
1144+35	5.7	43	0.12	11.48	0.46
1322+36	3.6	65	0.13	13.27	0.54
1339+26	6.8^p	90	0.08	7.97	0.32
1346+26	6.1	20	0.18	18.00	0.73
1357+28	5.0	40	0.07	6.63	0.27
1422+26	4.0	143	0.05	4.88	0.20
1441+26	unr.	...	0.03	3.26	0.14
1557+26	6.7	90	0.09	9.08	0.37
1652+39	...	173	0.09	9.45	0.38
1658+30	6.9^p	143	0.11	10.68	0.43
1752+32	5.5	92	0.06	6.33	0.26
1833+32	3.4	122	0.10	9.69	0.39
1855+37	unr.	...	0.02	1.65	0.67
2116+26	unr.	...	0.03	2.64	0.11
2236+35	unr.	...	0.04	3.86	0.16
2320+32	2	116	0.09	9.03	0.37
2335+26	2^p	100	0.04	4.39	0.18

[a] p indicates a galaxy pair.

Viegas & de Gouveia Dal Pino 1992). Another possibility is addressed by Baum et al. (1995). They suggest that the observed difference between PRGs and WRGs are due to structural properties of the central engines.

5.4. *Global Properties of WRGs*

In Paper I, we used V, R, and I optical images to classify the galaxies by their interaction degree in groups A and B which show obvious signs of interaction and group C that includes non-interacting elliptical or disk galaxies. The properties of each group and sources in the WRG sample, based on V, R, and I data from Paper I, are

- Group A. Sources with two nucleus within 15 kpc or connected to another galaxy by a gas bridge: B2 0055+25, B2 0120+33, B2 0838+32, B2 0913+38, B2 0916+33, B2 1346+26, B2 1752+32, B2 2116+26, B2 2236+35, B2 2320+32, B2 2335+26.

- Group B. Sources associated with another galaxy of comparable size and in a common halo: B2 0116+31, B2 1339+26, B2 1658+30.

- Group C. Sources without obvious features of interaction: B2 0034+25, B2 0331+39, B2 1116+28, B2 1144+35, B2 1322+36, B2 1357+28, B2 1422+26, B2 1441+26, B2 1557+26, B2 1652+39, B2 1833+32, B2 1855+37.

Based on the EELR results presented in Figs. 1*a* and 1*b*, we can revise the interactive features of group C galaxies. Most have complex or non-elliptical structures (filaments or extensions) indicating possible interaction features. Even B2 1116+28 and B2 1652+39, which show roughly elliptical contours, have an indication of distorted outer contours. This

TABLE 5

OPTICAL AND RADIO LUMINOSITIES[a]

Source B2	$L_{H\alpha}$	L_{radio}^{total}	L_{radio}^{core}
0034+25	41.31	1.22	0.55
0055+26	29.10	47.79	0.96
0116+31	91.01	53.54	274.50
0120+33	75.39	8.12	0.20
0331+39	5.67	3.07	3.26
0838+32	30.05	38.86	27.04
0913+38	6.07	18.15	2.71
0916+33	99.13	4.16	...
1116+28	90.26	20.83	7.16
1144+35	55.39	5.73	53.23
1322+36	74.01	2.29	2.46
1339+26	26.70	26.11	13.97
1346+26	136.30	55.25	11.39
1357+28	18.48	4.33	6.58
1422+26	10.03	12.11	1.84
1441+26	4.46	11.14	0.15
1557+26	34.71	2.14	3.25
1652+39	37.57	8.80	76.15
1658+30	47.96	8.36	5.55
1752+32	16.87	2.82	1.30
1833+32	39.45	205.90	34.63
1855+37	1.15	10.67	16.35
2116+26	2.94	0.38	0.68
2236+35	6.28	2.59	...
2320+32	34.31	0.29	...
2335+26	8.11	80.11	13.12

[a] In units of 10^{39}erg s^{-1}.

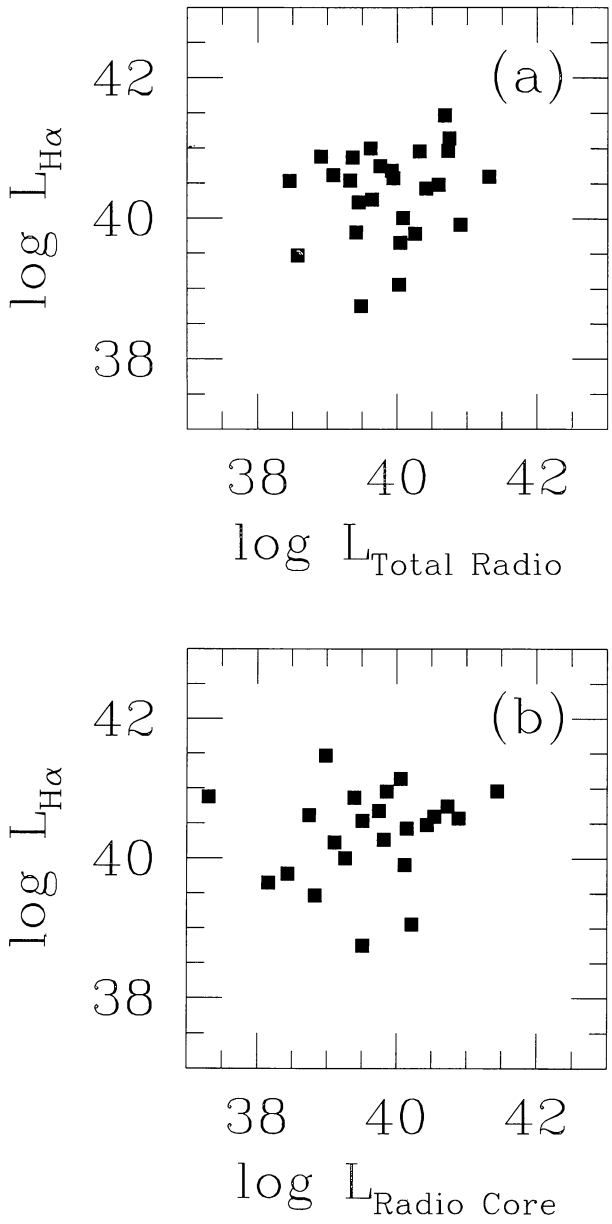

Fig. 5(a). Plot of log L_{radio}^{total} and log $L_{H\alpha}$ for WRGs. (b). Plot of log L_{radio}^{core} and log $L_{H\alpha}$ for WRGs.

result indicates that also in galaxies with no apparent interaction features as shown in the V, R, and I images of Paper I, the observed extended emission-line gas is distorted and has a complex structure and that they should probably be classified as members of Group A. We conclude that the majority of the WRGs studied here (80–90%) show strong or weak signs of interaction.

To see if the interaction degree is reflected in the physical parameters of the emission-line gas, we present in Table 6 the mean Hα luminosity, sizes of both the EELR and the radio features (jets, lobes, halos) and mean values for the electron density, mass and ionization parameter of the emitting gas.

We found that groups A and B (with obvious interaction features in V, R, and I images) have n_e, M_{gas} and U somewhat higher than group C (no interaction in V, R, and I images). Group A and C parameters are quite similar, except M_{gas} which is significantly lower in group C. Group B galaxies stand out in Hα and radio luminosities and in sizes of the emitting region. These results can be interpreted in the following scheme: sources from group A have had an interaction in the past, galaxies from group B are interacting or had a recent interaction, and group C emission is produced by weak interaction or shocks with the ambient medium around the nuclear region. If this scenario is correct, the bulk of the emission gas was acquired by galaxy interactions, where at least one galaxy was necessarily gas rich, in order to explain the high luminosities observed at Hα.

TABLE 6

EXTENDED EMISSION-LINE GAS IN WRG GROUPS

Type	L_{radio} (10^{40} erg s^{-1})	$L_{H\alpha}$ (10^{40} erg s^{-1})	R_{radio} (kpc)	R_{EELR} (kpc)	n_e (cm^{-3})	M_{gas} (10^9 $M_\odot$)	U (10^{-2})
Group A	2.28	4.04	36.14	4.18	0.10	1.01	0.45
Group B	2.93	5.52	64.65	5.77	0.11	1.11	0.45
Group C	2.40	3.39	29.18	4.33	0.08	0.79	0.37

5.5. *General View of Radio Galaxies*

In a similar manner to the classification of Fanaroff & Riley (Fanaroff & Riley 1974; Bridle & Perley 1984) for radio emission, FRI and FRII, Smith & Heckman (1989a,b), Baum & Heckman (1989a,b) have proposed a classification in the optical: Type A (FRII) and Type B (FRI). In this scenario our results can complete the characteristics of Type B radio galaxies:

Type A: Galaxies with radio structure of type FRII, with low optical luminosity (Smith & Heckman 1989a,b), in low-middle galaxy density environments (Prestage & Peacock 1988), with intense lines in emission (Heckman et al. 1986), with morphological peculiarities $\sim$ 56% indicatives of mergers between galaxies (Heckman et al. 1986; Baum & Heckman 1989a,b; Smith & Heckman 1989), and abnormal colors, bluer compared to normal elliptical galaxies of similar morphological type (Smith & Heckman 1989a,b). The blue colors can be caused by starbursts and the mergers between galaxies, where at least one is a spiral galaxy (rich in gas), and can be the origin of the ionized gas in the EELR. The occurrence of an EELR in Type A galaxies, is $\sim$ 85% with typical radius of $\sim$ 10 kpc. This EELR have oval morphologies and in some cases filaments are observed (Baum et al. 1988; Baum & Heckman 1989a). These galaxies are detected at 25, 60, and 100 μm, with mean luminosity $L_{FIR} \sim 1.7 \times 10^{10}\ L_\odot$ (Heckman et al. 1994). The luminosities in Hα, FIR, and radio are higher than Type B sources due to a more energetic nuclear process. The correlation between L_{radio}^{total} and $L_{H\alpha}$ has a slope 0.75 $\pm$ 0.09 (Zirbel & Baum 1995).

Type B: Galaxies with radio structure FRI, have elliptical morphology, although some are spiral and peculiar galaxies. These galaxies are in middle-high galaxy density environments, $\sim$ 29% are associated to clusters or groups of galaxies (Paper I). About 65% have morphological peculiarities, that are indicative of interactions. These galaxies also have bluer colors, similar to Type A galaxies. The EELR are resolved in $\sim$ 81% of these galaxies, with mean size of 4.6 kpc and oval morphologies with central condensations (this paper) that usually show distortions in the outer parts, probably due to galaxy interactions. In the infrared, they are detected at 12, 60, and 100 μm, with a mean luminosity $L_{FIR} \sim 7 \times 10^9\ L_\odot$ (Heckman et al. 1994). The luminosities in Hα, FIR, and radio are lower than Type A sources due to a less energetic nuclear process. The correlation between L_{radio}^{total} and $L_{H\alpha}$ has a slope 0.22 $\pm$ 0.07 (this paper).

As has been discussed above, these results show that the differences between powerful and weak radio galaxies are basically quantitative. In all radio galaxies, the central source is responsible for all degrees of activity in scales up to 10 kpc. Extended emission-line gas is observed associated to the surrounding medium around the nuclear region, with strong similarities in weak and powerful sources. The galaxy environment is important since interactions and mergers are more likely in high-galaxy density regions and gas can be acquired from interaction with a gas-rich companion, but it probably plays a secondary role in the development of EELRs. Finally, the unique sequence that would naturally link Type A to Type B and a large variety of powerful and weak AGNs (Figures 6 and 7) comparing Hα and radio luminosities has to be studied further incorporating more weak sources in the studies.

6. INDIVIDUAL GALAXIES RESULTS

A brief description of the extended emission-line regions in the individual galaxies studied here is presented in this section, which includes the observed properties in Hα+[N II] and/or [O III], and in some galaxies a comparison to the radio and optical broad-band morphology.

B2 0034+25. Galaxy with EELR detected both in Hα+[N II] and [O III], with oval morphology, size of $\sim$ 3.2 kpc and PA = 3°. A tongue is seen at PA = 160° which is the main orientation of the galaxy major axis in R. Radio jets (Fanti et al. 1986) lie perpendicular to the EELR, which is mainly associated to the radio core.

B2 0055+26 (NGC 326). Pair of galaxies in a common halo, both galaxies have small oval EELRs of equal intensities with a mean size of 6.2 kpc and oriented E–W. Extended radio emission (Ekers et al. 1978) is associated to the NW galaxy.

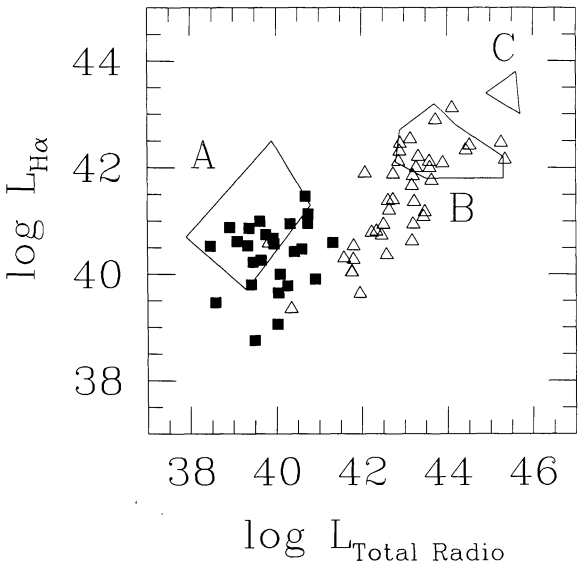

Fig. 6. Plot of log L^{total}_{radio} and log $L_{H\alpha}$ for different types of AGNs: □ our sample of WRG; △ PRG (Baum & Heckman 1989a); (A) region of Seyfert galaxies (Whittle 1985; de Bruy & Wilson 1978); (B) the zone of steep-spectrum quasars (Stockton & Mac Kenty 1987), and (C) region of high redshift radio galaxies (Spinrad 1987).

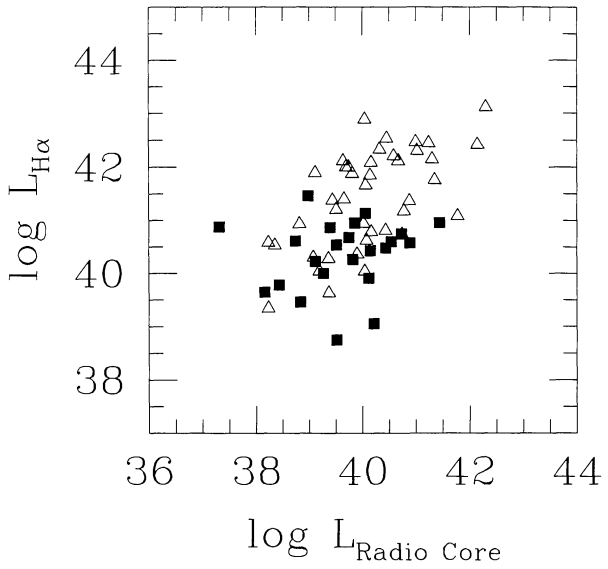

Fig. 7. Plot of log L^{core}_{radio} and log $L_{H\alpha}$ for our sample of WRGs (□) and PRGs (△) (Baum & Heckman 1989a).

B2 0116+31 (4C 31.04). Galaxy pair in a common halo. The brighter galaxy has an EELR with elliptical morphology, with size of 3.6 kpc and a PA of 79°, which is different to the optical PA, and is associated to the unresolved core radio source (Fanti et al. 1987) and host galaxy nucleus.

B2 0120+33 (NGC 507). Galaxy with an elliptical EELR that has a secondary peak to the south, PA = 21° and size of 2 kpc. The major axis of EELR lies close to galaxy major axis (9°) but not to the radio jet (90°, de Ruiter et al. 1986).

B2 0331+39 (4C 39.12). The EELR is complex, with size of 3 kpc and looks like a shell with an extension at 170° and another at 240°. The south-eastern extension coincides with the radio jet orientation, EELR lies inside the radio structure (Parma et al. 1986).

B2 0838+32 (4C 32.26). EELR shows a complex structure, with the main emission associated to the brightest member of a group of 4 galaxies. The Hα structure delineates the modification of the main galaxy contours at the positions of the other three galaxies. The EELR is possibly associated to the brighter radio source of the two detected by de Ruiter et al. (1986).

B2 0913+38. Galaxy with an EELR centrally condensed with 5 kpc in size. The observed structure has a box-like shape with elongation from northwest to southeast (PA = 155° and 335°) and from north-east to southwest (PA = 55° to 235°). The EELR shows similar morphology as the external part of the galaxy at R. The EELR lies inside the radio structure possibly associated with the core source (Fanti et al. 1978), but it is also unclear due to the complexity of the radio lobes which shows several knots along the E–W direction (Parma et al. 1986), two of which lie at the border of the EELR.

B2 0916+33. Spiral galaxy with two nuclei, line-emission is observed associated to both with PA = 137°. The EELR that corresponds to the brighter nucleus has a size of 4.6 kpc and a PA = 137° and no radio jet has been reported, only a core source (Colla et al. 1975b).

B2 1116+28. Galaxy with an almost circular EELR centrally condensed. Associated to the central radio source of an extended structure at PA = 80° (Fanti et al.1978).

B2 1144+35. Galaxy with an elliptical EELR, with a size of 5.7 kpc and a PA of 43°, shows a weak extension towards the W. The radio jet (Parma et al. 1986) lies at PA = 120° and the EELR is associated to a region around the core radio source with no emission or extension in the jet direction.

B2 1322+36 (NGC 5141). Galaxy with elliptical EELR centrally condensed oriented in the E–W direction and extending 3.6 kpc, to the E and W extensions delineate a weak S-shape. The radio structure has also an "S" shape oriented N–S (Fanti et al. 1986), with the EELR associated to the internal part of the double-jet.

B2 1339+26 (4C 26.41). Radio galaxy pair (wide-angle tail radio galaxy to the NW and head-tail radio galaxy to SE, Parma et al. 1986) with an EELR

of 6.8 kpc associated to each source, being brighter on the SE source which is also centrally concentrated. The morphology of the EELR shows distortion in the outer contours ("C" shape), probably due to the galaxy interaction. No clear association of EELR to the stellar distribution at R. The EELR of the SE source is associated to the central source of the radio structure that extends to the NE at PA$\sim$ 25° while the NW part lies close to the separate radio core source to the NW.

B2 1346+26 (4C 26.42). cD galaxy in the cluster Abell 1795, with X-ray emission (Jones et al. 1979) and two internal radio lobes with "S" shape in N–S direction (Bridle & Fomalont 1978) and two optical lobes at Hα with similar shape as the radio lobes (van Breugel et al. 1984) but smaller in size. We found a similar structure at Hα to van Breugel et al. (1984). The [O III] image presented here is spatially coincident with the Hα emission and shows similar morphology. In Fig. 4, the spatial coincidence of radio and optical emission are illustrated by superimposing on the [O III] image the radio structure at 6 cm (Bridle & Fomalont 1978) and the dust lane found by Pinkney et al. (1996). It is clear that the core radio source lies in the bridge between the two lobes, the NE radio lobe coincides remarkably well with the [O III] gas distribution. The southern ionized gas is almost twice more extended in the E–W direction than the radio continuum emission. The maximum of the [O III] emission is associated with the external eastern part of the radio lobes, maybe indicating that in this region the radio jet and the ambient galaxy are producing strong shocks that enhance the ionized gas emission. The dust lane traces the edge of the NE radio lobe and also the edge of the [O III] emission, and the absorption produces a hole in the [O III] emission to the west of the core. The existence of a dust lane might explain the weakness and smaller size of the [O III] emission associated to the NE lobe.

B2 1357+28. Galaxy with an EELR centrally concentrated oval structure with size of 5 kpc and a filamentary structure to the SE. The EELR coincides with central part of the N–S radio structure (Fanti et al. 1978).

B2 1422+26. Galaxy with an elliptical EELR, with size of 4 kpc and PA of 140°. The EELR seems associated with the central part of the radio emission lobes (de Ruiter et al. 1986).

B2 1441+26. EELR unresolved, probably associated to the core source of the two-lobe radio structure (de Ruiter et al. 1986).

B2 1557+26. EELR with a boxy structure with size of 6.7 kpc and oriented E–W in the external part but N–S in the internal part. The radio structure is oriented E–W (Fanti et al. 1978).

B2 1652+39 (4C 39.49). Source associated to BL Lac object (MK 501) with an unresolved radio source (Fanti et al. 1987). We found a rather compact EELR centrally condensed and oriented almost N–S (PA = 170°) close to galaxy major axis (131°).

B2 1658+30 (4C 30.31). Galaxy pair in a common halo with an EELR associated to the brighter galaxy at V. The EELR has a complex structure, maybe conical in the southern part, with its brightest region associated to the central source of a complex radio structure (Fanti et al. 1978), that has a jet at PA = 235° and radio lobes to the NE and SE. The EELR shows emission in the direction of the radio lobes but of smaller length, and a knot is observed towards the jet. The EELR size is 6.9 kpc with PA $\sim$ 143°.

B2 1752+32. Galaxy pair in a common halo, the EELR is associated to the brightest galaxy with size of 5.5 kpc and PA of 92°, an eastern extension is observed associated to the companion. A double radio jet extends from the NE to the SE (Parma et al. 1987) and the EELR is associated to the central region.

B2 1833+32 (3C 382). The EELR shows a centrally concentrated S-shape structure, with size of 3.4 kpc and main orientation at PA = 122°. The radio structure is complex, it shows two lobes oriented to the NE and SW (Parma et al. 1986), with the EELR associated to the SW lobe.

B2 1855+37. EELR unresolved associated to the unresolved radio core (Parma et al. 1986).

B2 2116+26. EELR unresolved associated to the radio core of 2-jet structure oriented N–S (Parma et al. 1986).

B2 2236+35. EELR unresolved associated to the core of two lobe radio structure (Parma et al. 1986).

B2 2320+32. Peculiar galaxy with a rather complex and interesting EELR with a 2 kpc size. At least 5 knots are observed in Hα, the structure in [O III] shows a central source associated to the galaxy central region and a C-type tongue to the SE also seen in the R image. The radio structure of this source is unknown and only a radio continuum source is detected (Colla et al. 1975a).

B2 2335+26 (NGC 7720). Galaxy pair with a common halo in the cluster Abell 2634, possibly a cD galaxy. The brighter galaxy has an EELR with size of 2 kpc and PA = 100°. Line-emission is also detected from the companion. Radio emission lobes are seen at 158 kpc in a C-shape, the EELR is associated to the central radio core (van Breugel 1980).

7. CONCLUSIONS

In this paper, we present the results of a program of optical observations in the narrow-band filters Hα+[N II] $\lambda\lambda$6548,6583 and [O III] λ5007, of a sample of 26 weak radio galaxies. The main results can be summarized as follows:

1. Spatially extended emission-line gas is quite

common in weak radio galaxies. Line emission is detected in all the sources in the sample and 81% of them have resolved emission-line nebulae.

2. The mean size of the EELR is $\sim$ 4.6 kpc and the mean emission-line luminosity in Hα+[N II] or [O III] is $\sim 1.1 \times 10^{41}$ erg s^{-1}. The latter is one order of magnitude greater than the luminosity of emission-line nebulae in normal early-type galaxies and similar to that of powerful radio galaxies.

3. The emission-line nebulae of WRGs have morphologies similar to those in PRGs. In some sources we observe only small, centrally condensed, kpc scale regions with elliptical or oval forms, in others we detect external distortions as tongues or filaments and in a few much more extended filaments several kpc from the host galaxy nucleus are detected.

4. Estimates of the density and total mass of the emission-line gas, assuming case B recombination, yield values from 0.01 to 0.26 cm^{-3} and 1.16×10^8 to 2.63×10^9 $M_\odot$, respectively. These values are similar to those of powerful radio galaxies.

5. From the correlation found between Hα and radio luminosities, we propose that the central source is also the source of ionization of the EELR in WRGs. The dispersion in this correlation may be produced by shocks between radio jets and the intergalactic gas and dust from the host galaxy.

6. Since most galaxies have interaction features and the ionized gas properties (n_e, M_{gas}, U, and $L_{\mathrm{H}\alpha}$) are enhanced by the interaction degree, we suggest that the emission gas in WRGs was acquired by mergers/collision between galaxies, where at least one galaxy was rich in gas.

7. The EELR in weak radio galaxies brighter spots or condensations are associated to the core radio source and located in the nuclear region of the host galaxy.

8. With these results, we proposed that the central source (maybe a black hole), in both weak and powerful radio galaxies, is the direct responsible for the ionization up to scales of 10 kpc, and that the properties of the host galaxy and the galactic environment play a secondary but important role, since they provide the ambient gas.

We thank L. A. Martínez for support in the computation facilities at the IAUNAM and for his invaluable help with the reduction software packages. Our very special thanks to the OAN/SPM team of night assistants: G. García, S. Monroy, J. Velazco, and F. Montalvo; and to the technical support group, whose help and assistance is greatly appreciated. Our thanks to the referee whose comments improved our presentation. This project has been partially supported by grants IN300789 and IN501694 (DGAPA, UNAM).

REFERENCES

Baum, S. A., & Heckman, T. 1989a, ApJ, 336, 681
_____. 1989b, ApJ, 336, 702
Baum, S. A., Heckman, T., Bridle, A., van Breugel, W., & Miley, G. 1988, ApJS, 68, 643
Baum, S. A., Zirbel, E. L., & O'Dea, P. 1995, ApJ, 451, 88
Bridle, A. H., & Fomalont, E. B. 1978, AJ, 83, 704
Bridle, A. H., & Perley, R. A. 1984, ARA&A, 22, 319
Brocklehurst, M. 1971, MNRAS, 153, 471
Capetti, A., Morganti, R., Parma, P., & Fanti, R. 1993, A&AS, 99, 407
Carrillo, R., Cruz-González, I., & Guichard, J. 1997, RevMexAA, 33, 31 (Paper I)
Colla, G., Fanti, C., Fanti, R., Gioia, I., Lari, C., Lequeux, J., Lucas, R., & Ulrich, M. H. 1975a, A&A, 38, 209
Colla, G., et al. 1975b, A&AS, 20, 1
Cornell, M. E., Aaronso, M., Bothun, G., & Mould, J. 1987, ApJS, 64, 507
Costero, R., & Osterbrock, D. E. 1977, ApJ, 211, 675
de Bruy, A. G., & Wilson, A. S. 1978, A&A, 53, 93
de Ruiter, H. R., Parma, P., Fanti, C., & Fanti, R. 1986, A&AS, 65, 111
Ekers, R. D., Fanti, R., Lari, C., & Parma, P. 1978, Nature, 276, 588
Fabbiano, G., Fassnacht, C., & Trinchieri, G. 1994, ApJ, 434, 67
Fanaroff, B. L., & Riley, I. M. 1974, MNRAS, 167, 31
Fanti, C., Fanti, R., de Ruiter, H .R., & Parma, P. 1986, A&AS, 65, 145
Fanti, C., et al. 1987, A&AS, 69, 57
Fanti, R., Gioia, I., Lari, C., & Ulrich, M. H. 1978, A&AS, 34, 341
Hansen, L., Nørgaard-Nielson, H. U., & Jørgensen, H. E. 1987, A&AS, 71, 465
Heckman, T. M., O'Dea, C. P., Baum, S. A., Laurikainen, E. 1994, ApJ, 428, 65
Heckman, T., Smith, E. P., Baum, S. A., van Breugel, W. J. M., Miley, G. K., Illingworth, G. D., Bothun, G. D., & Balick, B. 1986, ApJ, 311, 526
Jones, C., Mandel, E., Schwarz, J., Forman, W., Murray, S. S., & Harnden, F. R. 1979, ApJ, 243, L21
Kent, S. M. 1984, ApJS, 56, 105
Koski, A. T. 1978, ApJ, 223, 56
Lucy, L. B. 1974, AJ, 79, 745
Morganti, R., Fanti, C., Fanti, R., Parma, P., & de Ruiter, H. R. 1987, A&A, 183, 203
Morganti, R., Ulrich, M.-H., & Tadhunter, C. N. 1992, MNRAS, 254, 546
Oke, J. B. 1974, ApJS, 27, 21
Osterbrock, D. E., & Miller, J. S. 1975, ApJ, 197, 535
Parma, P., de Ruiter, H. R., Fanti, C., & Fanti, R. 1986, A&AS, 64, 135
Parma, P., Fanti, C., Fanti, R., Morganti, R., & de Ruiter, H. R. 1987, A&A, 181, 244
Pinkney, J., et al. 1996, ApJ, 468, L13
Pogge, R. W. 1989, ApJ, 345, 730
Prestage, L., & Peacock, J. 1988, MNRAS, 230, 131
Richardson, W. H. 1972, J. Opt. Soc. Am., 62, 52
Smith, E. P., & Heckman, T. M. 1989a, ApJS, 69, 365
_____. 1989b, ApJ, 341, 658
Spinrad, H. 1987, preprint

Stockton, A., & Mac Kenty, J. W. 1987, ApJ, 316, 584
van Breugel, W. 1980, A&A, 88, 248
van Breugel, W., Heckman, T., & Miley, G. 1984, ApJ, 276, 79
van Breugel, W., Miley, G., Heckman, T. M., Butcher, H., & Bridle, A. 1985, ApJ, 290, 496
Viegas, S. M., & de Gouveia Dal Pino, E. M. 1992, ApJ, 384, 467
Whittle, M. 1985, MNRAS, 213, 33
Zirbel, E. L., & Baum, S. A. 1995, ApJ, 448, 521

René Carrillo and Irene Cruz-González: Instituto de Astronomía, UNAM, Apartado Postal 70-264, 04510 México, D.F., México (rene,irene@astroscu.unam.mx).
José Guichard: Instituto Nacional de Astrofísica, Optica y Electrónica, Apartado Postal 216, 72000 Puebla, Pue., México (jguich@inaoep.mx).